KfK 3950
September 1985

XPS and EPXMA Investigation and Chemical Speciation of Aerosol Samples Formed in LWR Core Melting Experiments

H. Moers, H. Jenett, R. Kaufmann,
H. Klewe-Nebenius, G. Pfennig, H. J. Ache
Institut für Radiochemie
Projekt Nukleare Sicherheit

Kernforschungszentrum Karlsruhe

KERNFORSCHUNGSZENTRUM KARLSRUHE

Institut für Radiochemie
Projekt Nukleare Sicherheit

KfK 3950

XPS and EPXMA Investigation and Chemical Speciation of Aerosol Samples Formed in LWR Core Melting Experiments

H. Moers, H. Jenett, R. Kaufmann, H. Klewe-Nebenius,
G. Pfennig, and H.J. Ache

KERNFORSCHUNGSZENTRUM KARLSRUHE GMBH, KARLSRUHE

Kernforschungszentrum Karlsruhe GmbH
ISSN 0303-4003

ABSTRACT

Aerosol samples consisting of fission products and elements of light water reactor structural materials were collected during simulating in a laboratory scale the heat-up phase of a core melt accident. The aerosol particles were formed in a steam atmosphere at temperatures between 1200 and 1900 °C of the melting charge. The investigation of the samples by use of X-ray photoelectron spectroscopy (XPS) permitted the chemical speciation of the detected aerosol constituents silver, cadmium, indium, tellurium, iodine, and cesium.

A comparison of the elemental analysis results obtained from XPS with those achieved from electron probe X-ray micro analysis (EPXMA) revealed that aerosol particle surface and aerosol particle bulk are principally composed of the same elements and that these compositions vary with release temperature. In addition, quantitative differences between the composition of surface and bulk have only been observed for those aerosol samples which were collected at higher melting charge temperatures.

In order to obtain direct information on chemical species below the surface selected samples were argon ion bombarded. Changes in composition and chemistry were monitored by XPS, and the results were interpreted in light of the effects, which were observed when appropriate standard samples were sputtered.

XPS- und EPXMA-Untersuchung und chemische Speziation von Aerosolproben aus LWR Kernschmelzexperimenten

ZUSAMMENFASSUNG

Während der Simulation eines Kernschmelzunfalls eines Leichtwasserreaktors im Labormaßstab wurden Aerosolproben der freigesetzten Materialien gesammelt. Die Aerosolpartikel wurden in einer Wasserdampfatmosphäre gebildet, wobei die Temperatur des Schmelzgutes von 1200 - 1900 °C variierte. Dieser Temperaturbereich entspricht der Aufheizphase eines Kernschmelzunfalls. Die Untersuchung der Aerosolproben durch Röntgenphotoelektron-Spektroskopie (XPS) erlaubte die chemische Charakterisierung der Aerosolbestandteile Silber, Cadmium, Indium, Tellur, Iod und Cäsium.

Ein Vergleich der Elementanalyse aus XPS-Messungen mit den Resultaten der Elektronenstrahl-Röntgenmikroanalyse (EPXMA) zeigte, daß Oberfläche und "Bulk" der Aerosolteilchen prinzipiell aus den gleichen Elementen zusammengesetzt sind und daß diese Zusammensetzungen mit der Freisetzungstemperatur variieren. Zusätzlich wurden quantitative Unterschiede zwischen Oberfläche und "Bulk" nur bei solchen Aerosolproben beobachtet, die bei höheren Schmelzguttemperaturen gesammelt wurden.

Um direkte Informationen über chemische Spezies unter der durch XPS untersuchbaren Oberflächenschicht zu erhalten, wurden ausgewählte Proben durch Argonionenbeschuß oberflächlich abgetragen. Änderungen in Zusammensetzung und Chemie der Proben wurden anhand von XPS-Spektren verfolgt. Die Ergebnisse wurden interpretiert unter Berücksichtigung von Effekten, die sich beim Sputtern geeigneter Standardproben ergaben.

CONTENTS

INTRODUCTION

Considerations on the accident risks of nuclear power plants normally include the discussion of a highly improbable event: the meltdown of the reactor core which might occur after a loss-of-coolant accident with subsequent failure of the emergency core cooling system (1). The core meltdown will be accompanied by the release of various core constituents, i.e. fission and activation products and inactive structural materials. This release will take place in either gaseous form (e.g. noble gases) or as aerosol particles, which result from vaporization and recondensation of part of the core constituents (2).

Knowledge about the composition of the aerosols and especially the chemical speciation of their constituents is important in order to estimate the hazard potential caused by a hypothetical LWR core meltdown. In this context elements of radiological importance (e.g. iodine and cesium) are of special interest.

X-ray photoelectron spectroscopy (XPS) is an analytical technique, which allows elemental analysis and also chemical speciation, the latter being a consequence of varying chemical shifts of the photoelectron and Auger electron kinetic energies of different compounds of the same element (3,4,5). Furthermore, the information depth of XPS is only a few nanometers, making it sensitive to the outermost sample surface layer. XPS has been widely applied to the investigation of aerosol samples of different origin (5b, 6-11) making use of the possibility of chemical speciation, which is only of limited availability by other methods.

Electron probe X-ray micro analysis (EPXMA), in contrast, collects information from a region of about one micrometer thickness and can, therefore, be used to perform an elemental bulk analysis of the sample (12,13). Depending on the instrumentation it has the feature of investigating single aerosol particles of a size in the micrometer range (8) or to perform an integral elemental analysis of aerosol samples.

The present work shows the results of the investigation of a series of aerosol samples generated in separate core melting experiments (14,15,16). The surface chemistry was determined by XPS, and the bulk composition was evaluated from EPXMA measurements. Aerosols provide a relatively large surface compared to their volume, which increases the importance of surface effects during their formation. To reveal these differences the results of XPS and EPXMA were compared.

In an additional attempt to overcome the lack of depth information when using XPS, selected aerosol samples were argon ion bombarded to evaluate depth profiles of these samples. The profiles were compared with EPXMA results, too. The XPS spectra of aerosol particle surfaces after ion bombardment were evaluated under consideration of possible compositional and chemical changes, which might be introduced by the sputtering process.

EXPERIMENTAL

Details of equipment and experimental procedure for the simulation of a LWR core meltdown in a laboratory scale have been described elsewhere (14,15,16). The aerosol samples investigated in the present work were produced in a special run using inactive materials to avoid radioactive contamination of the XPS and EPXMA spectrometers. The composition of the starting material and the experimental conditions are summarized in Table 1.

Aerosol particles were collected on eight glass fiber filters (collection area $\simeq 63$ cm^2). The filters were charged subsequently for 150 seconds each over the temperature range given in Table 1. Table 2 lists the collected amount, melting charge temperature, and optical appearance of each aerosol fraction. The changes in color could not be attributed to chemical changes of the aerosol material, but were correlated with the collected amounts and thus with the thicknesses of the aerosol particle layers. Aerosol fraction no. 4 has been inadvertently charged too low during the meltdown experiment. This sample was included only to maintain the time sequence but its spectra were not evaluated further. The aerosol particles of the last fraction were collected at the end of the heating process, when the temperature inside the crucible already decreased. The size of the aerosol particles generated for the present work was not determined. It was concluded from other, similar core melting experiments that the size range was about 0.1 to 1 µm (15).

Elements and compounds, which were needed for standard measurements, were bought in highest purity commercially available from E. Merck AG, Darmstadt and Aldrich-Chemie GmbH & Co. KG, Steinheim and used without additional purification. Powder standard samples were measured as powder pellets of 10 mm diameter, which were produced at a pressure of 10^3 N mm^{-2}.

Aerosol samples were introduced into the spectrometers as small sections of the original glass fiber filters. These sections and also the standard samples were sticked to appropriate probes by use of adhesive silver paint.

Table 1: Conditions for Sample Generation

Simulated core:	90 g UO_2 including fission products [a]:		
	Cs:	3.7 10^{-1} wt %	(Cs_2CO_3, CsI)[b]
	I:	3.5 10^{-2} wt %	(CsI)[b]
	Ag:	8.3 10^{-3} wt %	(metal)[b]
	Cd:	1.3 10^{-2} wt %	(metal)[b]
	Te:	7.0 10^{-2} wt %	(metal)[b]
	In:	-	-
	51 g Zircaloy (98.5 wt % Zr; 1.5 wt % Sn)		
	100 g stainless steel		
	4.4 g neutron absorber (80 wt % Ag; 15 wt % In; 5 wt % Cd)		
Atmosphere:	steam; 130 °C; 2 bar		
Temperature range:	1200 °C - 1900 °C		

a) Amounts corresponding to a burn-up of 44.000 MWd/t uranium; all other fission products contained in adequate amounts were not detected by any of our methods and, therefore, left off the table.

b) Chemical form in the simulated fuel.

Table 2: Characteristic Parameters of Aerosol Fractions

No.	Melting Charge Temperature [°C][a)]	Collected Amount [mg]	Optical Appearance
1	1275	125	grey-brown
2	1480	78	bright brown
3	1630	110	brown
4	1720	7.4	b)
5	1810	113	brown
6	1900	185	dark brown
7	1900	371	black
8	1700	217	black

a) Temperature at the midpoint of the charging interval

b) Filter was irregularly charged; large part remained completely uncovered

XPS spectra were recorded in a Vacuum Generators ESCALAB 5 electron spectrometer at a base pressure of 10^{-9} mbar. Electrons were excited using unmonochromatized magnesium and aluminium $K\alpha$ radiation, and electron kinetic energies were measured with a hemispherical analyzer operated in the constant analyzer energy (CAE) mode. Overview spectra were recorded with a CAE of 50 eV, while elemental scans in the regions of main photo and Auger peaks were recorded with a CAE of 20 eV. The resolution of the spectrometer at 20 eV analyzer energy was determined for the 4f photopeaks of a cleaned gold sample to be 1.2 eV full width at half maximum (FWHM). Binding energies and kinetic energies of the aerosol constituents are given relative to the $3d_{5/2}$ photopeak of the silver component (binding energy of Ag $3d_{5/2}$ taken as that of the metal = 368.2 eV) or relative to the carbon 1s photopeak of the surface contamination (C 1s = 285.0 eV). Binding energies and kinetic energies of standard samples are referenced to the Au $4f_{7/2}$ = 84.0 eV (17). Photopeak intensities were determined from the peak areas after subtraction of the $K\alpha_{3,4}$ X-ray satellites (spacing and intensity relative to the main peak taken from Ref. 5a) and were corrected for calculated photoionization cross sections (18).

Photopeaks, which were composed of several components or which showed significant overlap, were evaluated by means of a curve synthesis program after subtraction of the $K\alpha_{3,4}$ X-ray satellites and the background of inelastically scattered electrons. The intensity of the background as a function of peak position and kinetic energy was determined using a mathematical formalism described in Ref. 19. The resulting difference spectrum was approximated by varying within reasonable limits kinetic energy positions, heights, and peak widths of an appropriate number of Gaussian peaks until the synthesized spectrum matched the difference spectrum with minimum rms deviation.

Argon ion bombardment of the samples was performed by sputtering the whole sample area with 5 keV Ar^+ ions, and XPS spectra were recorded after various sputtering times. The sputtering conditions were characterized by sputtering an anodically oxidized tantalum foil, where the same current density as applied to the aerosol samples yielded a sputtering rate of about 0.4 nm per minute.

EPXMA was performed in an International Scientific Instruments SMSM 1 scanning electron microscope with a lateral resolution of the secondary electron image of 0.1 µm. X-rays were excited on a sample area of about 3 mm^2 using 25 keV electrons, and X-ray energies were determined over an energy range of 1 to 10 keV using an energy dispersive spectrometer (Kevex µx 7000 Si(Li)

detector), which was attached to the scanning electron microscope. The energy resolution of the Si(Li) detector for X-rays between 3.0 and 5.5 keV was found to be 150 eV FWHM. Peak areas were determined for the main X-ray transition of each element observable in the given energy range ($K\alpha_{1,2}$ and $L\alpha_{1,2}$, respectively). $L\alpha_{1,2}$ peak intensities were corrected for different primary ionization rates using correction factors, which were calculated for pure elements relative to silver (cf. discussion).

RESULTS AND DISCUSSION

1. Elemental surface and bulk analyses

Figures 1 and 2 show XPS spectra measured for the aerosol samples no. 3 and no. 6 at melting charge temperatures of 1630 °C and 1900 °C, respectively. The surfaces of the eight aerosol sample fractions are composed of the elements silver, cadmium, indium, tellurium, iodine, cesium, oxygen, and carbon, the latter resulting from a surface contamination of the particles with carbon containing adsorbates (20,21). The composition changes markedly with melting charge temperature (cf. Fig. 6). There are no other elements detectable besides those listed above, except for sample no. 4, where in addition to the aerosol constituents silicon 2p and 2s photopeaks are observed, which must be attributed to the silicon constituent of the supporting glass fiber filter, visible due to the very low coverage of this filter (cf. experimental section).

Figures 3 and 4 show the corresponding EPXMA spectra of the samples no. 3 and no. 6, respectively. The spectra were recorded by exciting a fairly large sample area (≈ 3 mm^2) to yield an integral composition of the whole aerosol fraction and not that of single particles. This was due to the intention of obtaining comparable results for EPXMA and XPS, the latter yielding spectra from an excited area of about 50 mm^2.

In comparison to the XPS spectra significant differences are observed by EPXMA. Besides those elements, which were already detected by XPS, some of the aerosol samples (nos. 2-5) exhibit characteristic X-ray peaks from the glass fiber filter support. This is due to the much larger information depth of EPXMA and to the relatively poorer coverage of these samples compared to the others (cf. Table 2). Fig. 3 a shows the overall spectrum of sample no. 3. For comparison, Fig. 3 b shows the spectrum recorded for a clean, uncharged glass

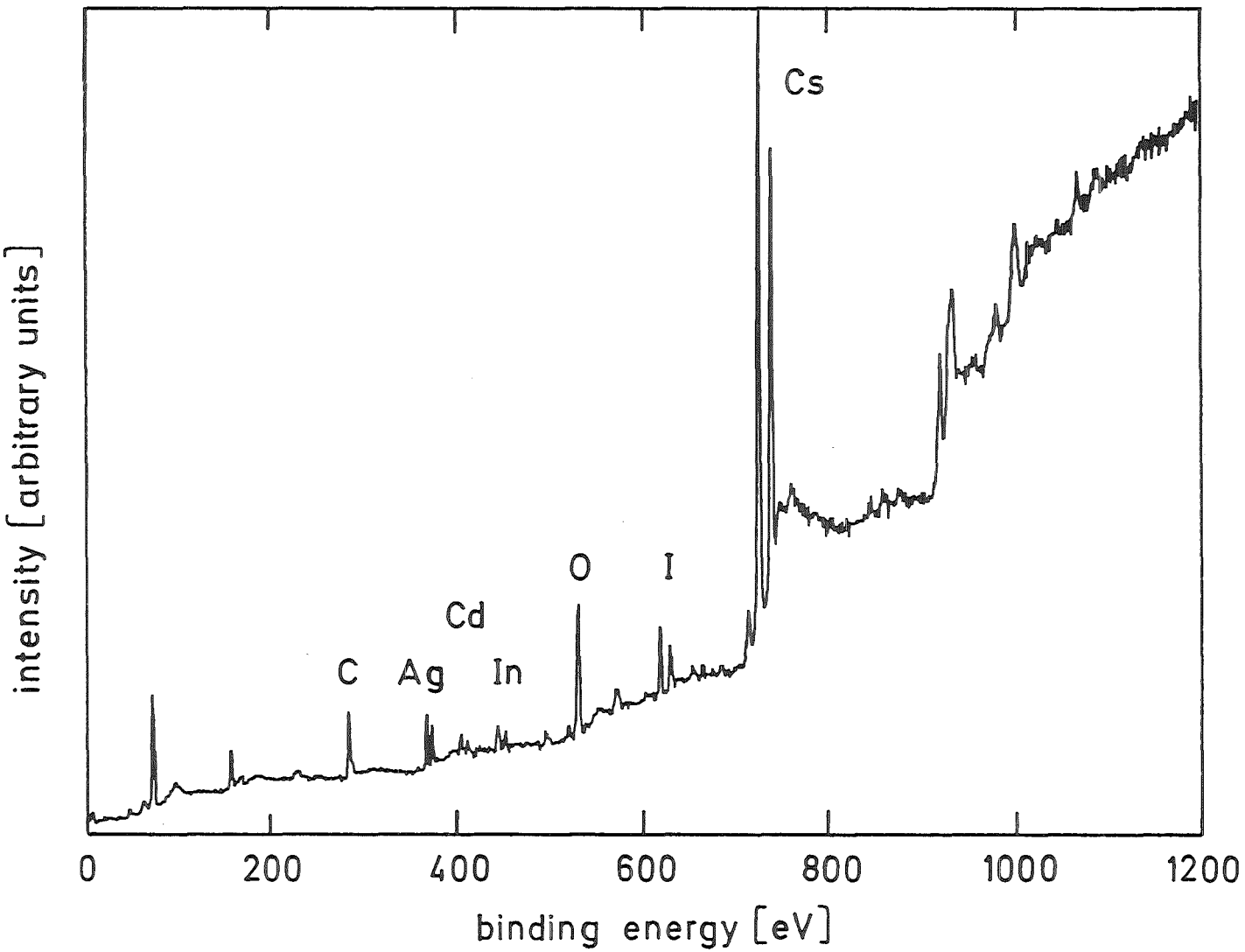

Fig. 1: XPS spectrum (AlK α) of aerosol sample no. 3 (melting charge temperature 1630 °C).

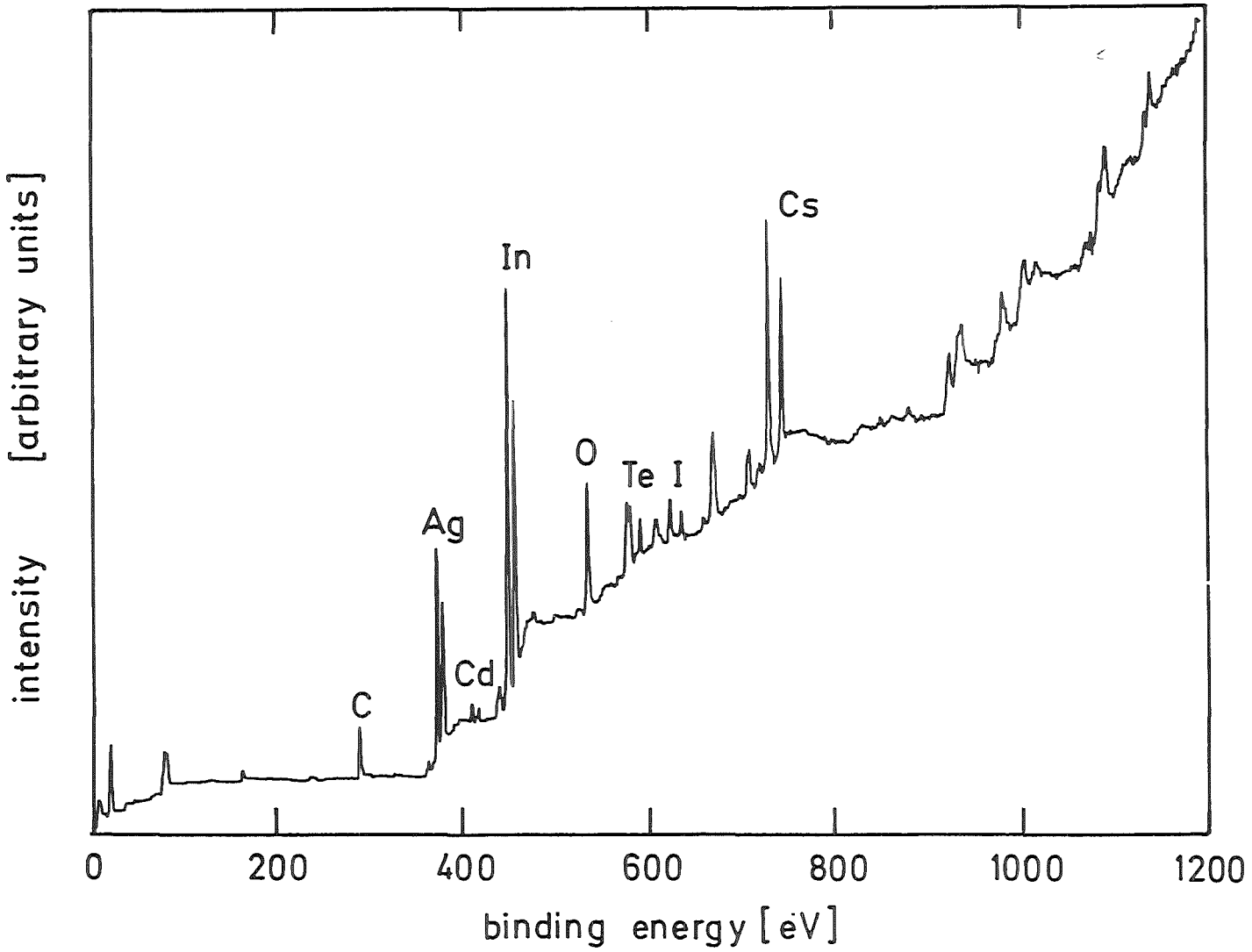

Fig. 2: XPS spectrum (AlK α) of aerosol sample no. 6 (melting charge temperature 1900 °C).

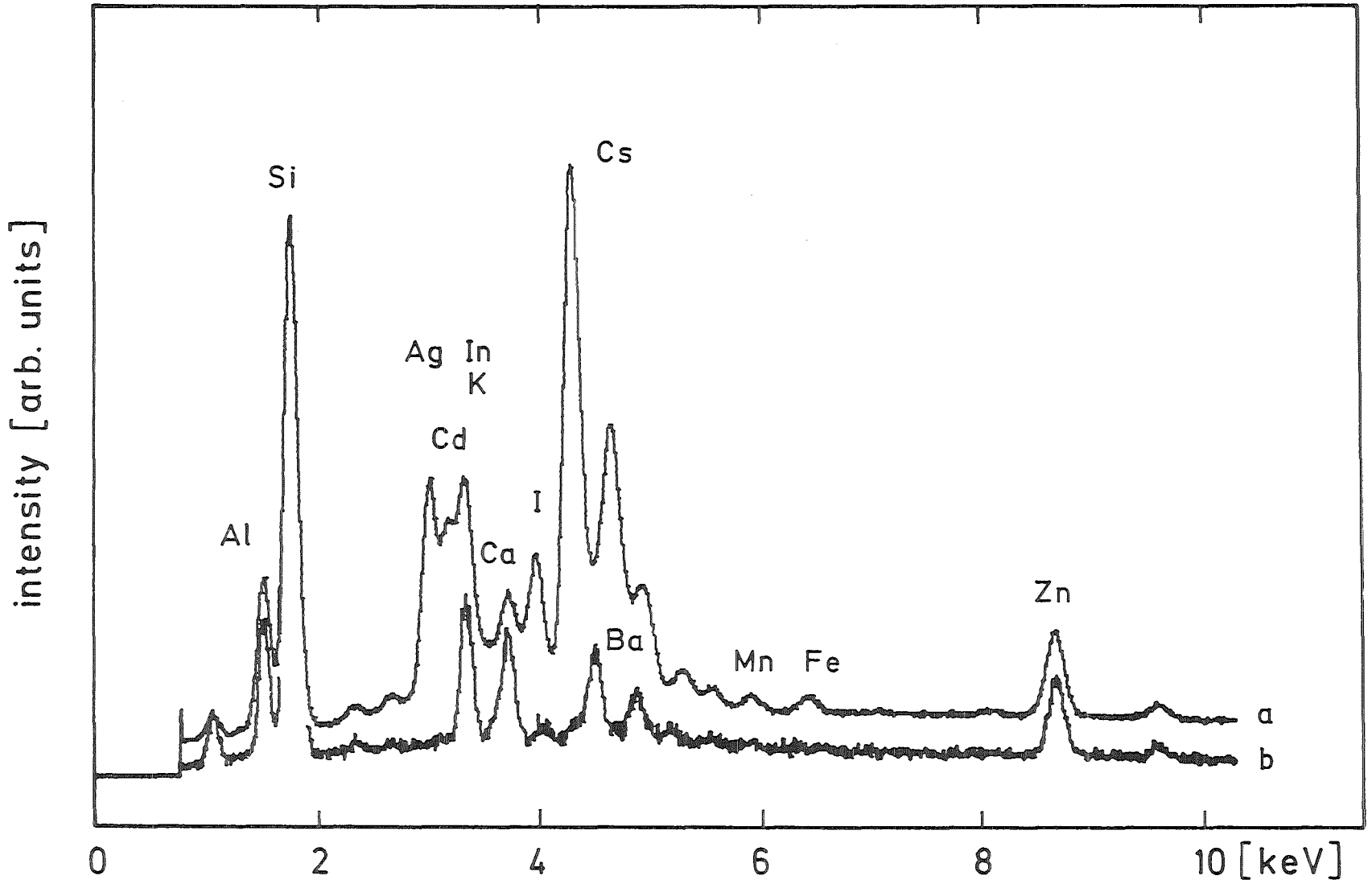

Fig. 3: a) EPXMA spectrum of aerosol sample no. 3 (melting charge temperature 1630 °C); b) EXPMA spectrum of an uncharged glass fiber filter.

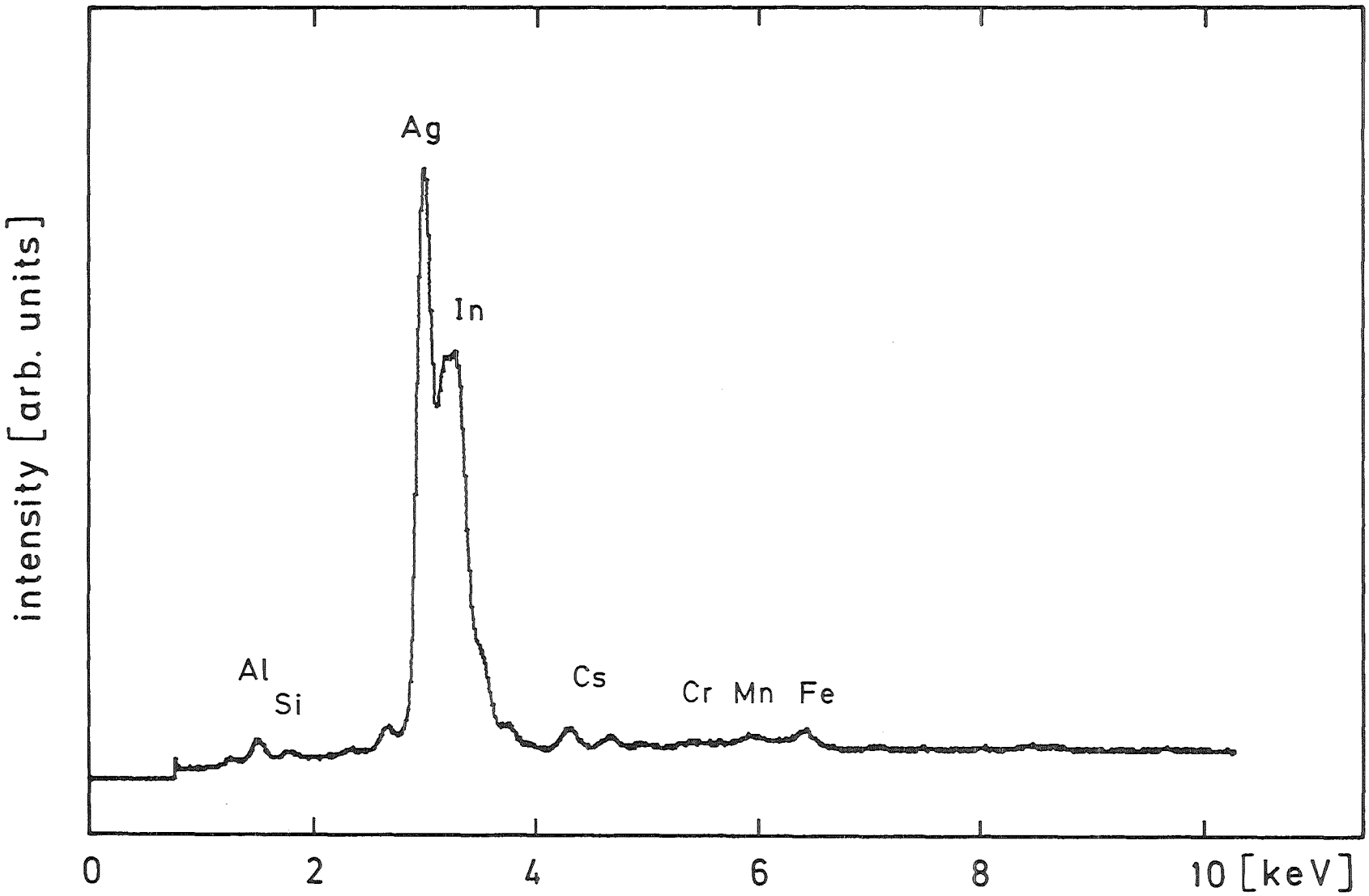

Fig. 4: EPXMA spectrum of aerosol sample no. 6 (melting charge temperature 1900 °C).

fiber filter showing the elements Al, Si, K, Ca, Ba, and Zn. The peaks of the glass fiber filter material are scaled to approximately the same height in both spectra. Fig. 4, in contrast, shows hardly any signals attributable to the support. Another difference in comparison to XPS results is the presence of characteristic X-ray lines of the transition metals iron, manganese, and chromium, which are observed in most of the samples, and which originate from the release of small amounts of the stainless steel component of the structural materials (cf. Table 1). Iron is not detected in the first sample only while manganese and chromium are observed in the samples nos. 3 to 7 and nos. 4 to 6, respectively. The relative intensities of their X-ray lines are in each case comparable to what is shown in Figures 3 and 4.

A general limitation in EPXMA is the difficulty of measuring elements with atomic numbers less than 11 (sodium; $E(K\alpha) = 1040$ eV) (13). This prevents us from a comparison of data of those elements with XPS data, which is especially important for oxygen ($E(K\alpha) = 525$ eV) and carbon ($E(K\alpha) = 277$ eV).

2. Comparison of surface and bulk composition

A comparison of XPS and EPXMA spectra going beyond a qualitative elemental analysis, needs reliable procedures to convert experimental elemental signal intensities into (relative) elemental concentrations. In principle, such procedures exist for both techniques, XPS (6,22,23,24) and EPXMA (12,13). However, depending on the analytical problem under consideration certain limitations have to be taken into account.

In XPS, the photoelectron peak intensity of an element in a thick, homogeneous sample can be approximated by (23):

$$I \propto N \cdot \sigma \cdot T \cdot \lambda \qquad (1)$$

where I is the measured intensity of the photoelectron peak, N is the number of atoms per cm^3, σ is the photoionization cross section of the photoelectron transition of interest, T is the transmission of the spectrometer, which is a function of the kinetic energy of the electrons (in the present case $T \propto E^{-1/2}$ (25)), and λ is the inelastic mean free path, which again is a function of kinetic energy (taken as $\lambda \propto E^{1/2}$, according to Ref. 26). Making use of the energy independence of the product $T \cdot \lambda$, the relative atomic concentrations of two

elements A and B in the same thick, homogeneous sample are derived as follows:

$$\frac{N_A}{N_B} = \frac{I_A \cdot \sigma_B}{I_B \cdot \sigma_A} \qquad (2)$$

Eqs. 1 and 2 do not take into account any anisotropy of the angular distribution of photoelectron emission. In addition, if concentration gradients exist in the probed sample layer, the experimentally observed signal intensities depend on the concentration profile of each element. The presence of any adsorptive contamination layer will introduce additional inaccuracy, if the photoelectron peaks, which are used for the determination of intensity I, differ in kinetic energy (23).

The applicability of Eq. 2 was tested using two compound standards, cesium iodide and silver iodide, which were selected since they cover the kinetic energy range of the XPS spectra of the aerosol constituents. The standards were measured several times, using a freshly prepared pellet for each measurement. The peak intensities of the surface contaminations carbon and oxygen were in each case less than 5 % of the I $3d_{5/2}$ peak intensiy. The stoichiometric ratios were calculated from the averaged intensities of the spin-orbit split 3d peaks. The σ-values for the 3 d levels were taken from the Scofield calculations (18). The measurements yielded atomic ratios (cation to anion) of 1.00 ± 0.04 (CsI) and 1.03 ± 0.03 (AgI). These results agreed reasonably well with the expected stoichiometric coefficient of each of the two compounds. Therefore, the signal intensities of the major photoelectron peaks of each element in the aerosol samples were normalized to the corresponding σ -values thus yielding relative atomic concentrations. Any other corrections, e.g. regarding concentration gradients, were not attempted due to the complexity of the aerosol samples. It will be shown lateron that, in part, such gradients exist, which consequently will falsify the results of the quantification.

The standard procedure for the quantitative evaluation of EPXMA spectra is based on the so-called ZAF (atomic number, absorption, fluorescence) correction, which consists of the comparison of the X-ray signal intensities of the sample and of (normally elemental) standards. The observed intensity ratio of sample and standard of each element has to be corrected for three effects (12,13d):

- Differences in the retardation of the incoming electrons and in the backscattering factors of standard and sample (atomic number correction).

- Differences in the absorption of primarily excited X-rays in standard and sample (absorption correction).

- Differences in the excitation of secondary fluorescence processes in standard and sample (fluorescence correction).

However, this procedure is strictly applicable only to solid samples of dimensions "infinite" in comparison to the volume analyzed by the primary electron beam. If the analysis is applied to single small particles of a diameter of a few micrometers or less, the actual volumes of the particles are influencing the sample signal intensities, and will, in principle, lead to a reduction of signal intensity with decreasing particle size (27,28). The same will hold of course, if the sample consists of a film thinner than the in-depth extension of the excitation volume of the primary electron beam. In both cases, the sample dimensions have to be known as an additional correction parameter.

As has been shown before, the glass fiber filters of the aerosol samples have not been charged equally (cf. Table 2). With regard to the foregoing comments it would be difficult to perform a standard ZAF correction, because the dimensions of the probed aerosol material differ from sample to sample and are, in addition, not known. However, an at least semiquantitative comparison of the concentrations of the main constituents of aerosol surface and bulk would be desirable. Therefore, the X-ray $L\alpha_{1,2}$ signal intensities of these elements were determined from the spectra. These experimental signal intensities were then corrected for different primary ionization rates to yield relative atomic concentrations using relative correction factors, which were calculated for pure elements according to Refs. 12 and 13a from the following equation:

$$I_q = k\, R_q\, \nu_q\, A_q^{-1}\, \omega_q\, (E_o\, E_{c,q}^{-1} - 1)^{1.67} \qquad (3)$$

In this formula I_q is the primary X-ray intensity of element q, A is the atomic weight, ω is the fluorescence yield, E_o is the primary energy of the ionizing electrons, and $E_{c,q}$ is the minimum "critical" energy of an electron to perform ionization in the given shell. The proportionality constant k is assumed to depend on the respective shell but not on atomic number. The electron backscattering

coefficient R was taken to be identical for all six elements, which can be verified in Ref. 13e, where the actual R values differ by only 2 %. The detection probability ν of the Si(Li) detector can be taken as unity in the energy range of interest (3.0 keV to 5.5 keV).

Table 3 lists the values used for the calculations, the calculated relative intensities of the $L\alpha_{1,2}$ transitions ($I_{Ag,rel} = 1$), and the resulting correction factors, by which the experimental $L\alpha_{1,2}$ peak intensities were multiplied.

The reliability of this approach was tested for thick samples by measuring EPXMA spectra of pure silver iodide and cesium iodide pellets and by determining from these spectra the apparent stoichiometry when the calculated relative sensitivity factors (Table 3) were used. Their characteristic X-ray lines cover the energy range of interest and the spectra, for that reason, allow to conclude on the influences of absorption and secondary fluorescence, which are neglected in this approach and which should cause deviations from the correct results if their relative contributions vary significantly from element to element and depending on the element combination.

The determination of the $L\alpha_{1,2}$ signal intensities from the spectra of the standards and of the aerosol samples was further complicated due to significant overlap of the multiple X-ray emission lines of different elements in the covered energy range (3.0 to 5.5 keV). The contribution of each element to the complex sample spectra was determined by using the shapes of single element spectra and varying their heights until the measured spectrum was reproduced with sufficient accuracy. The peak shapes were obtained from elemental samples or from simple compounds (e.g. AgI).

Fig. 5 illustrates the analysis procedure of the EPXMA spectra of the standard samples silver iodide and cesium iodide. The bremsstrahlung background was taken as a straight line. Fig. 5 a shows the spectrum of silver iodide. Both L series are represented by four Gaussian peaks each corresponding to the four observable, partly unresolved components of the L series of each element. The vertical bars indicate the peak heights h of the $L\alpha_{1,2}$ components. The peak height as a measure for the element concentration is approximately proportional to the peak area since the resolution of the detector is almost constant in the given energy range. The stoichiometry of this sample was calculated to be 0.97 by using the correction factors determined from Eq. 3.

Table 3: Values Used for Calculation in Equation 3, Calculated Relative Intensities $I_{q,rel}$ of L $\alpha_{1,2}$ Transitions and Correction Factors $(I_{q,rel})^{-1}$

q	A_q	ω_q (Ref. 13 b)	$E_{c,q}$ [keV] (Ref. 13 c)	$I_{q,rel}$	$(I_{q,rel})^{-1}$
Ag	107.9	0.047	3.350	1.00	1.00
Cd	112.4	0.050	3.537	0.92	1.09
In	114.8	0.054	3.730	0.88	1.14
Te	127.6	0.068	4.341	0.73	1.37
I	126.9	0.073	4.558	0.72	1.39
Cs	132.9	0.084	5.011	0.65	1.54

E_o = 25 keV; $I_{q,rel} = I_q \cdot I_{Ag}^{-1}$

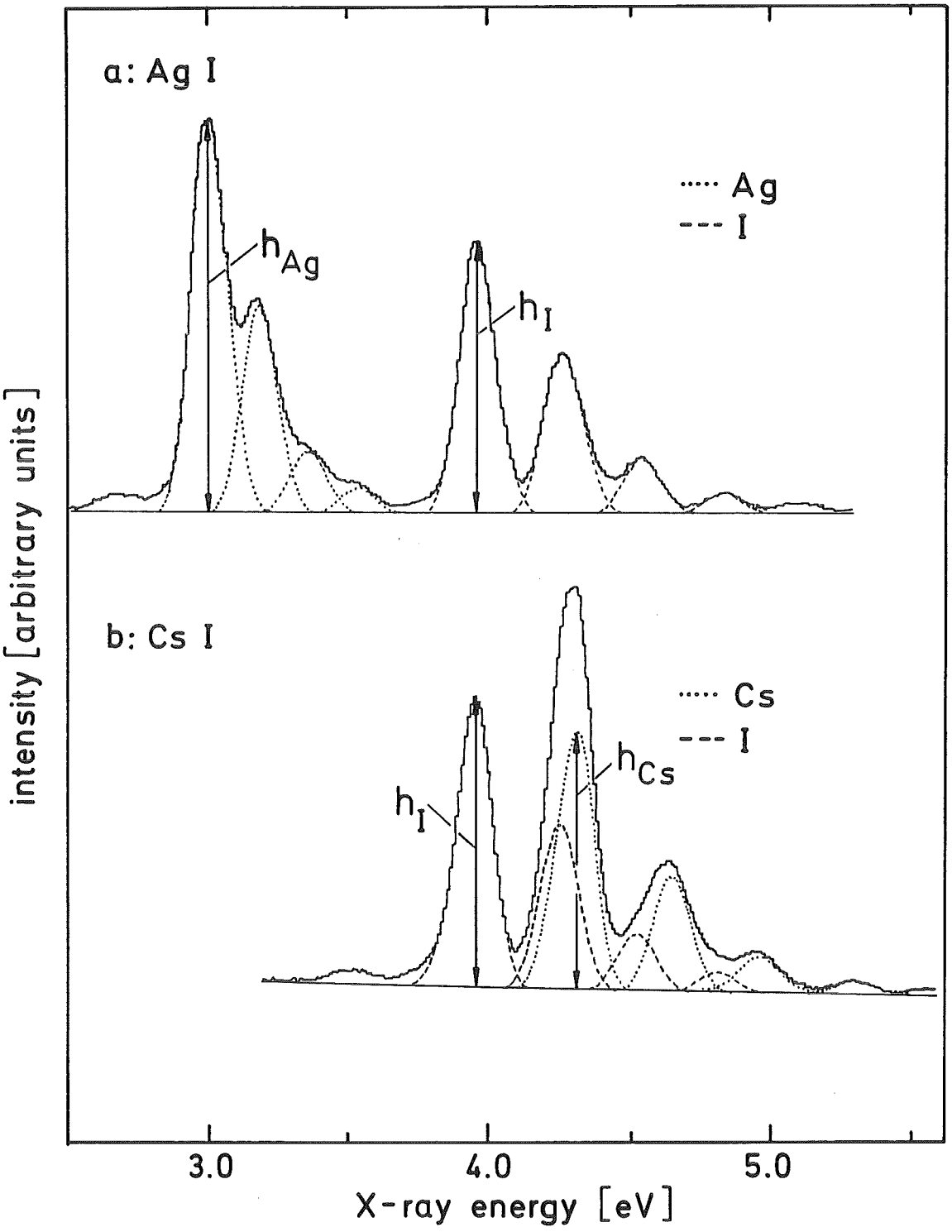

Fig. 5: EPXMA spectra of pure silver iodide and cesium iodide and multiplet analysis for the determination of the $L\alpha_{1,2}$ peak intensities. The vertical bars correspond to the $L\alpha_{1,2}$ peak heights (h), which are approximately proportional to the peak areas due to the only slight dependence of the analyzer resolution on X-ray energy.

Fig. 5 b shows the EPXMA spectrum of cesium iodide. The overlap of the cesium and iodine peak is significant. The result of the best fit procedure is shown in addition. The Gaussian peaks show the relative contributions and intensities of the iodine and cesium peaks in the original spectrum. In this case the stoichiometry was calculated to be 1.01.

The accuracy of this procedure applied to the two standard compounds was reasonable. Therefore, the same approach was used for the evaluation of the aerosol sample EPXMA spectra. However, it must be stated that the accuracy of this process decreases if the relative concentration of a given element is small or if a larger number of components is present. In fact, the accuracy of the best fit procedure should be limiting the achievable overall accuracy. We, therefore, believe that the results, which will be shown in the following section, are accurate to within 10 rel.-% for major components, but may differ from the real value by up to 50 rel.-% for minor components.

Fig. 6 summarizes the results of both described quantification procedures for the aerosol particle surface composition (upper diagram, from XPS measurements) and the aerosol particle bulk composition (lower diagram, from EPXMA measurements). The two diagrams include only those elements which could be detected by both techniques. Therefore, oxygen and carbon are not included in the upper part of the figure, even though both elements are present in significant amounts in the XPS spectra. One hundred atomic percent are thus represented by the sum of the atomic concentrations of the elements silver, cadmium, indium, iodine, tellurium, and cesium.

It can be seen from both diagrams that the composition of the aerosol particles as a function of melting charge temperature is governed by the volatilities of the elements. Highly volatile elements (cadmium from the neutron absorber, cesium and iodine as fission products) appear at lower temperatures, while less volatile elements (silver and indium from the neutron absorber) require higher temperatures for their release. The appearance of small amounts of indium already at relatively low melting charge temperatures is somewhat puzzling due to the low vapor pressure of indium metal at these temperatures. The general release behavior is similar in both diagrams. Differences arise for tellurium, which was not detected in the EPXMA spectra, and for the transition metals iron, chromium and manganese, which, vice versa, could not be detected in XPS spectra. This may be due to real differences in surface and bulk composition for these elements (which turned out to be the case for tellurium, see later). However, it has to be taken into account that the relative elemental sensitivities as a function of atomic number Z show a different behavior in XPS and EPXMA,

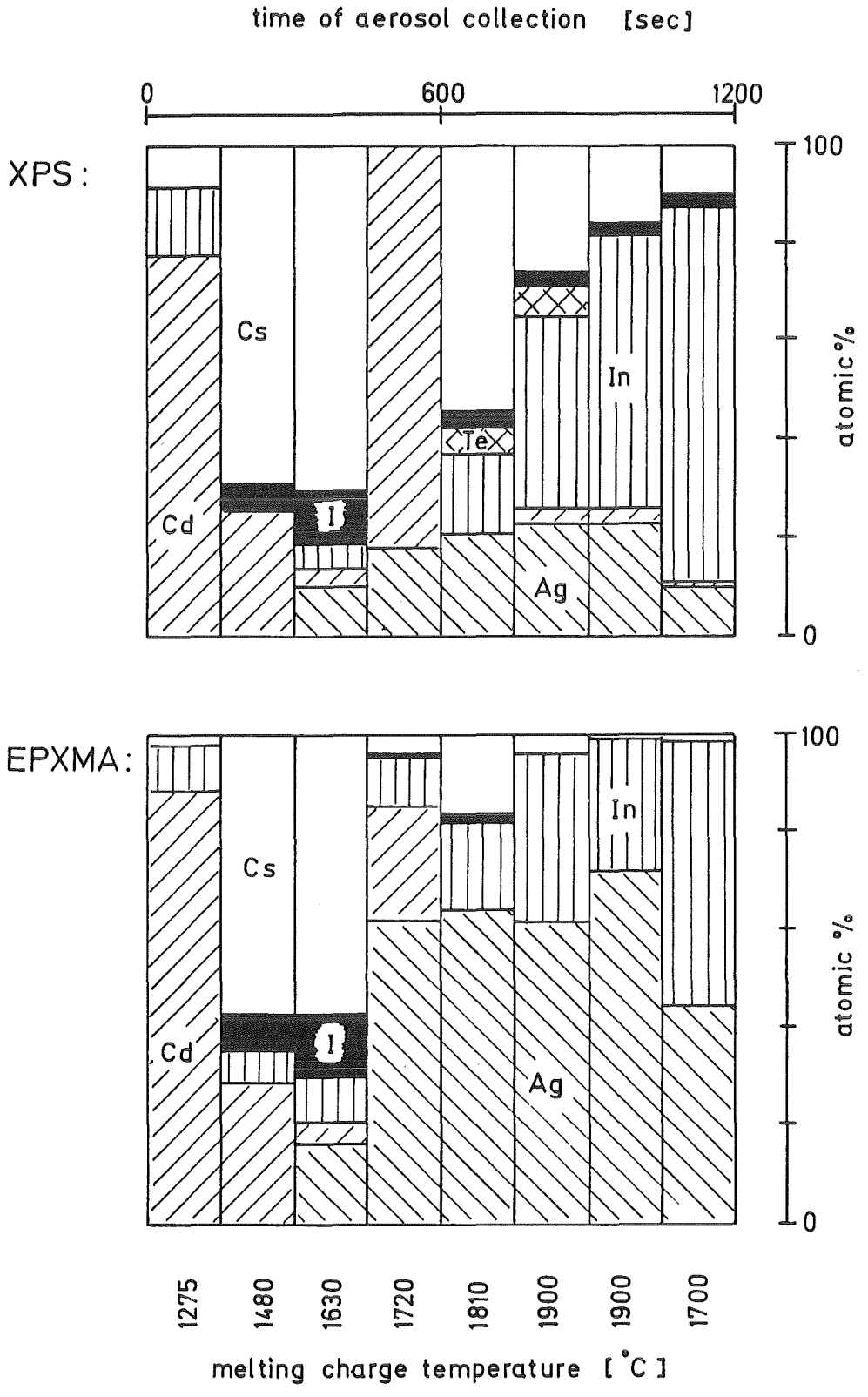

Fig. 6: Comparison of surface composition (XPS) and bulk composition (EPXMA) of the aerosol fractions. The aerosol fraction collected at 1720 °C has been inadvertently charged too low during the aerosol generation process and was, therefore, not used for data interpretation, but was only included in the figure to avoid a rupture in the time sequence.

respectively. At comparable photoelectron kinetic energies and characteristic X-ray energies, respectively, and if concentration gradients are absent, the element of higher atomic number Z is detected with larger probability in XPS while in EPXMA the element of lower Z is favored, especially if different electron shells are involved. This is shown in Table 4 for the example of chromium compared to tellurium. The relative sensitivities in XPS are taken to be identical to the relative photoionization cross sections (18) of the main photopeaks. Those of EPXMA were calculated using Eq. 3 and taking the values from Ref. 13 and a primary excitation energy of 25 keV. It can be expected from a comparison of the values in Table 4 and from the small amounts of iron, chromium, and manganese in the EPXMA spectra that these elements cannot be detected by XPS because their concentration will be below the detection limit of this technique unless a surface enrichment has taken place. In turn, the absence of XPS signals of iron, chromium, and manganese leads to the conclusion that these elements are bulk components rather than surface constituents. Based on similar considerations it can be estimated using Eq. 3 that iron, chromium, and manganese in total contribute to no more than about one atomic percent to the total composition. Therefore, they are not included in the lower diagram of Fig. 6.

Besides the qualitative differences discussed before additional ones with regard to the absolute atomic fractions are observed. At lower temperatures the compositions of aerosol particle surface and bulk are fairly identical. At higher melting charge temperatures EPXMA spectra show a significant enrichment of silver in the aerosol bulk while the surface shows a larger concentration of indium and cesium and the presence of iodine. These observations correspond to the enrichment of more volatile species on the aerosol particle surface.

In order to confirm the results of the XPS/EPXMA comparison, selected aerosol samples have been argon ion bombarded, and the resulting new surface has been measured by XPS. The results of this procedure are shown in Figs. 7, 8, and 9 corresponding to the aerosol samples 1, 3, and 6, respectively. The compositions of the aerosol sample surfaces resulting for various sputtering times are compared to the bulk composition of the same sample (from Fig. 6).

The elemental surface composition of sample no. 1 is nearly not changed independent of sputtering time (Fig. 7) and is well comparable to what is observed for the bulk. In contrast, if aerosol sample no. 6, for which significant differences between surface and bulk have been observed, is sputtered, the composition as viewed by XPS is changed markedly (Fig. 9). The amounts of

Table 4: Relative Elemental Sensitivities S_{rel} of Chromium and Tellurium in XPS and EPXMA

	XPS		EPXMA	
	photopeak (binding energy)	S_{rel}	X-ray peak (energy)	S_{rel}
Cr:	$2p_{3/2}$ (≈580 eV)	1	$K\alpha_{1,2}$ (≈5410 eV)	1
Te:	$3d_{5/2}$ (≈580 eV)	2.4	$L\alpha_{1,2}$ (≈3770 eV)	0.2

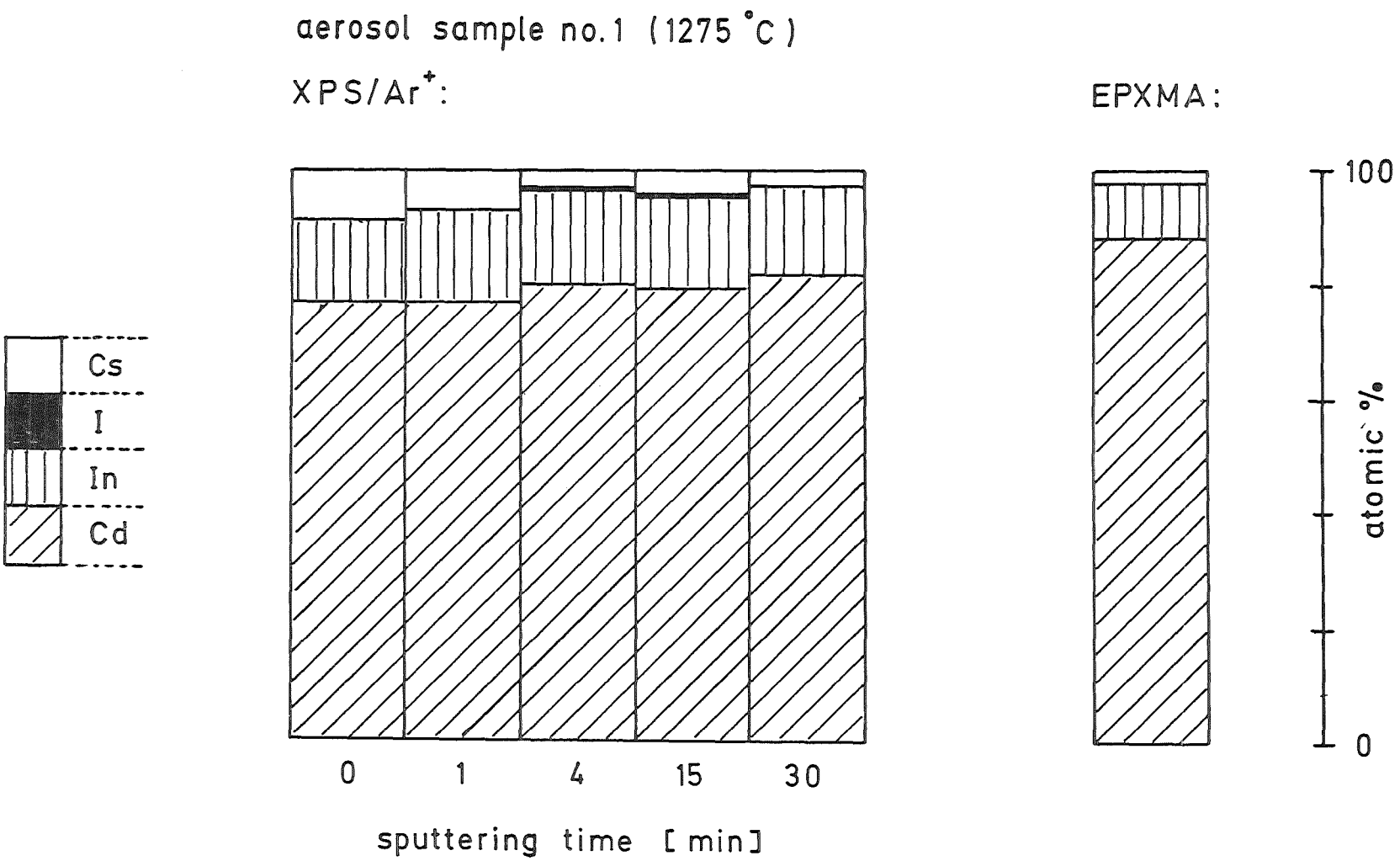

Fig. 7: Comparison of the surface composition after various sputtering times and the bulk composition from EPXMA measurements of aerosol sample no. 1 (melting charge temperature 1275 °C).

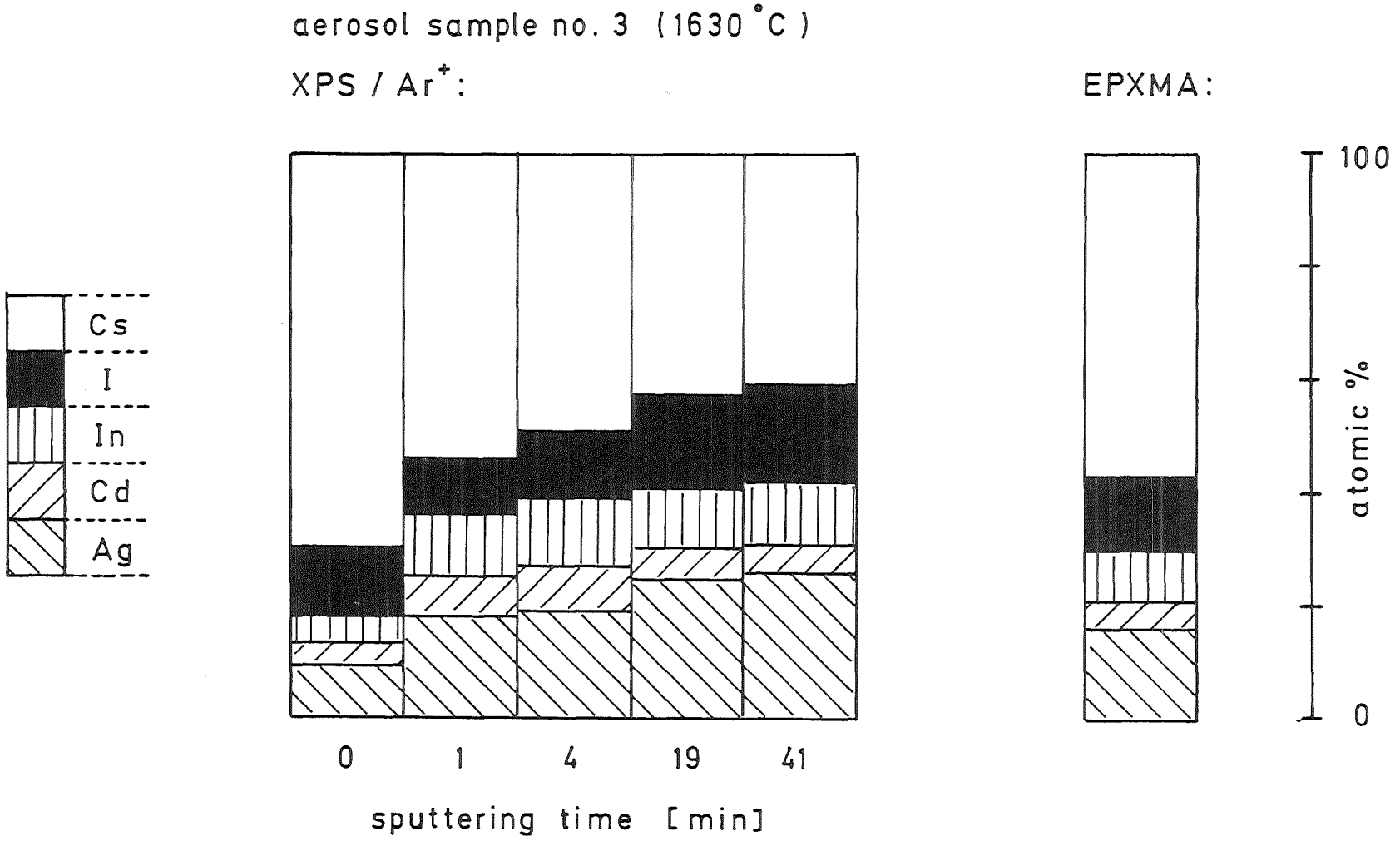

Fig. 8: Comparison of the surface composition after various sputtering times and the bulk composition from EPXMA measurements of aerosol sample no. 3 (melting charge temperature 1630 °C).

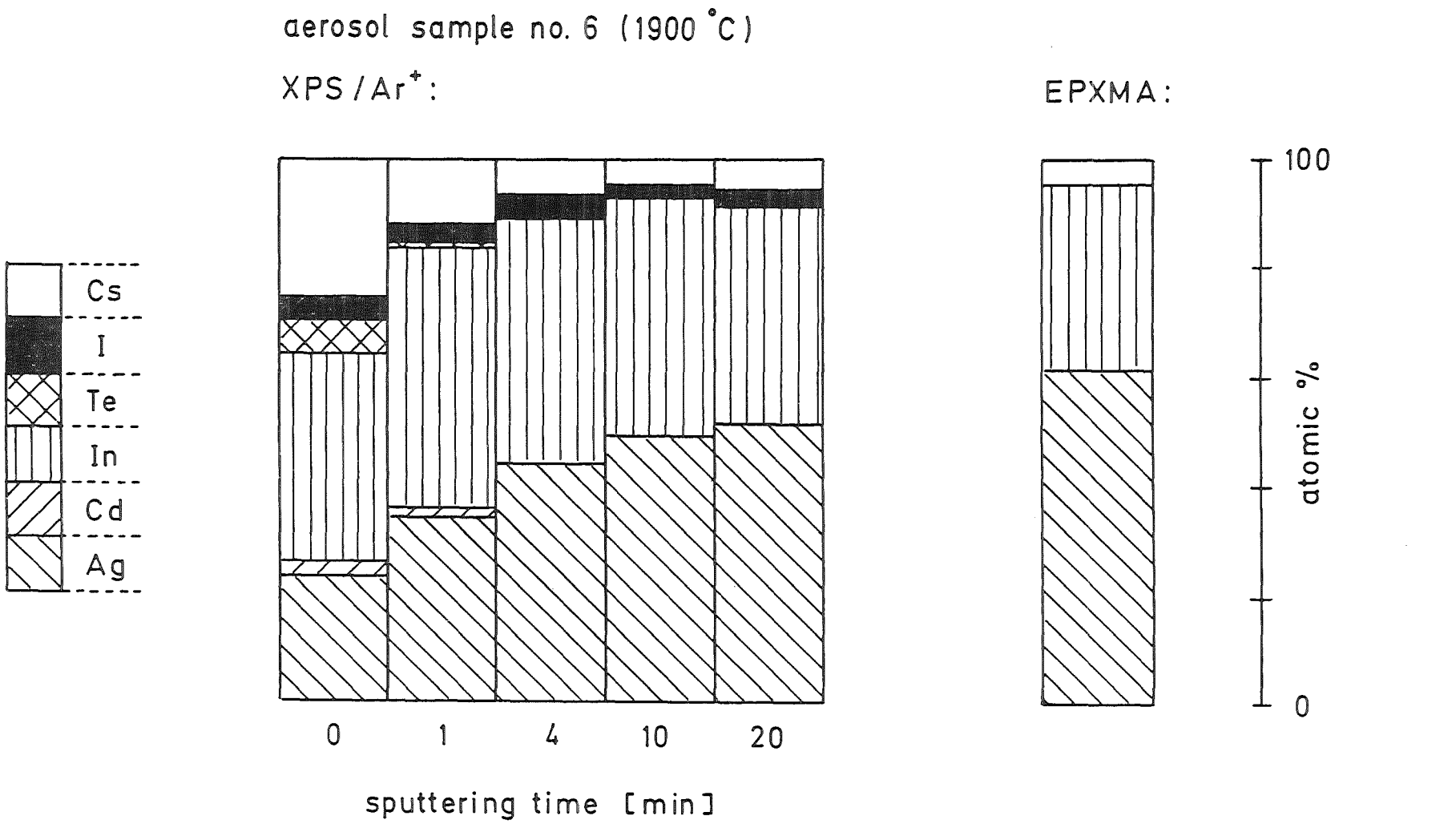

Fig. 9: Comparison of the surface compositions after various sputtering times and the bulk composition from EPXMA measurements of aerosol sample no. 6 (melting charge temperature 1900 °C).

cesium, tellurium and cadmium are reduced heavily after one minute of ion bombardment indicating a surface enrichment of these elements. Parallel to the increasing sputtering time the contributions of the main constituents of this sample, indium and silver, also change their relative concentrations until a composition is reached, which is similar to that of the bulk. In both cases the sputtering experiments confirm the conclusions drawn from Fig. 6.

However, contradictory observations are made for aerosol sample no. 3 (Fig. 8). Without sputtering the surface composition is almost identical to what is observed for the bulk. Sputtering leads to a depletion of cesium compared to all other constituents and thus to an apparent difference of the bulk composition as viewed by EPXMA and XPS combined with argon ion bombardment, respectively. However, we believe that this discrepancy can be explained by the actual sample composition and the effect of the sputtering process on it.

According to Kelly (29) the sputtering process can be subdivided into three single processes: collisional sputtering, prompt thermal sputtering, and slow thermal sputtering. The latter two processes are described as a vaporization due to a shortly lived high temperature in the region of ion impact and as a vaporization of target elements at ambient temperature after bombardment induced decomposition, respectively. Both effects will increase the sputtering yield above its level from pure collisional sputtering. As a criterion for the existence of prompt thermal sputtering a vapor pressure around 100 atm at a temperature of 3000 to 4000 K was stated (29). As will be shown in the following sections cesium is present in the aerosol samples as hydroxide. Its thermodynamic data (30,31) fulfil the criterion given above. In addition, it can be expected that cesium hydroxide is decomposed by sputtering so that also contributions of slow thermal sputtering will be present. In view of these purely qualitative arguments we conclude that the experimentally observed relative decrease of the cesium concentration is due to preferential sputtering because of thermal sputtering effects and is not a feature of the sample in-depth composition. That the loss of cesium occurs as cesium hydroxide can be seen from the XPS spectra which show a parallel loss of oxygen and cesium with increasing sputtering time. Unfortunately, a direct evidence from experimental data on the sputtering yields of cesium hydroxide or closely related compounds is not avaiblable, to our knowledge.

3. Chemical speciation

Chemical speciation is based principally on the determination of the binding energy position of the main photopeak, of the kinetic energy of a selected Auger transition, and of the modified Auger parameter, which is defined as the sum of binding energy and kinetic energy of selected, normally predominant, photo- and Auger electron peaks, respectively (32). These three parameters are then compared to the corresponding ones of appropriate reference elements or compounds. Additional, complementary information can be achieved in the case of compounds, if the bonding partner(s) is (are) included in the data evaluation.

3.1 General results

The results of the chemical speciation of the major surface constituents of the aerosol samples have already been reported (20) as has the chemical speciation of iodine (21). These results are only summarized briefly to maintain a complete presentation and due to the need of these results in the following discussion. It has been shown, based on the spectral energies of the metal components that silver is present as metal while the other elements cadmium, indium, tellurium, and cesium are found in oxidized states as either oxides (In, Te) or hydroxides (Cd, Cs). The well defined chemical state of silver and its presence in most of the samples allowed to use it as internal standard to correct the experimentally observed electron kinetic energies for charging of the samples (20,21).

It is interesting to compare these results with the XPS spectra of oxygen of the different aerosol fractions. Fig. 10 shows four XPS spectra of the O 1s photoelectron peak recorded for the aerosol samples nos. 1, 3, 6, and 7. The two arrows on top of the spectra indicate the approximate positions on the binding energy scale of oxide and hydroxide oxygen. The binding energy spacing between the two states has been taken from literature (33-36) and from own measurements to be about 2 eV. The spectra indicate that the first and the third aerosol fraction consist mainly of hydroxides while the lower spectra (corresponding to the samples nos. 6 and 7) are representative for oxides. A comparison with the aerosol composition given in Fig. 6 (upper part) shows that the hydroxide components must be cadmium hydroxide (sample no. 1) and cesium hydroxide (sample no. 3), respectively. The small shoulder on the low binding energy side of the uppermost spectrum in Fig. 10 can in part be attributed to the smaller indium oxide contribution.

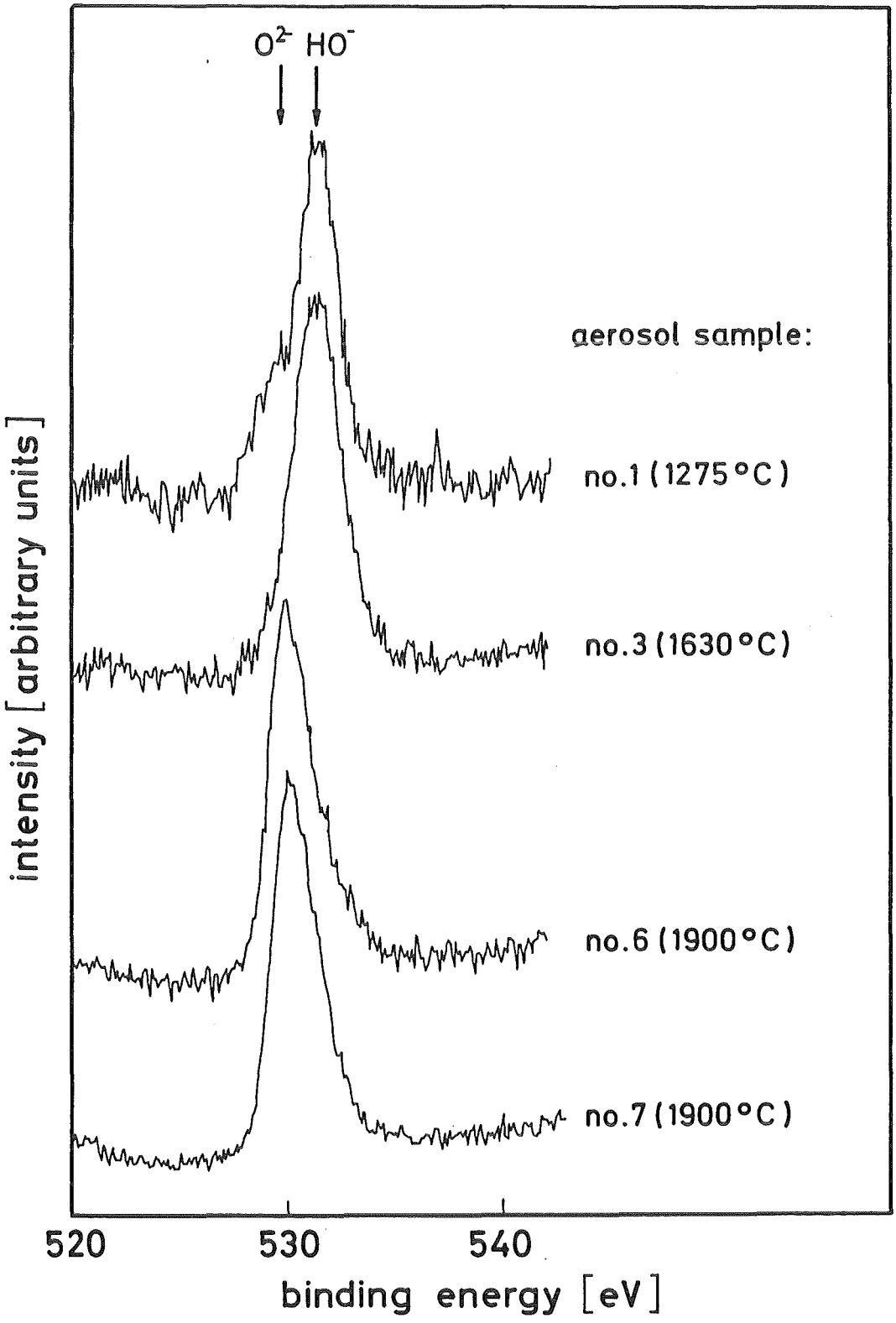

Fig. 10: XPS O 1s spectra of four aerosol samples collected at different melting charge temperatures. The arrows on top indicate the approximate binding energy positions of oxide and hydroxide O 1s photopeaks.

At high melting charge temperatures where the aerosol particles are mainly composed of indium and silver, the oxide peaks originate essentially from indium oxide since silver has been proven to be present as metal (20). The asymmetry of the O 1s peaks on the high binding energy side of the two lower spectra indicates the additional presence of some hydroxide in these samples.

The chemical speciation of iodine has been evaluated from the spectral parameters of the aerosol sample with the highest iodine contents (no. 3) before and after sputtering of the sample with argon ions (21). It has been concluded that iodine is bound mainly to cesium but that a small amount is also bound to silver.

The XPS results on chemical speciation presented above are strictly seen only valid for the aerosol particle surface region. This limitation can be overcome by using argon ion bombardment to remove surface near sample material and to provide a new surface for XPS measurements. However, sputtering is not necessarily an "inert" technique, and surface alterations under the influence of ion bombardment have to be taken into account.

The following chapters describe the chemical changes observed for the samples nos. 1 and 6 after sputtering. While compositional changes have already been described in the context of the comparison of surface and bulk composition, chemical changes are discussed with regard to differences in surface and bulk chemistry of the aerosol particles. Possible changes induced by the argon ion bombardment were monitored by bombarding appropriate standard compounds under as far as possible identical conditions.

3.2 Details of cadmium speciation

Fig. 11 shows XPS spectra of sample no. 1 after inelastic background and X-ray satellite subtraction in the binding energy region of the Cd 3d and O 1s photopeaks. The upper spectra correspond to the original surface composition (Fig. 11 a). The Cd 3d peaks are asymmetric with a tailing on the low binding energy side and can each be resolved into two components with about one eV spacing as shown by the four Gaussian peaks, which reproduce the total peak envelope. The asymmetry cannot originate from inhomogeneous sample charging since indium and cesium exhibit 3d peaks of purely Gaussian shape. The O 1s peak is clearly consisting of at least two contributing species.

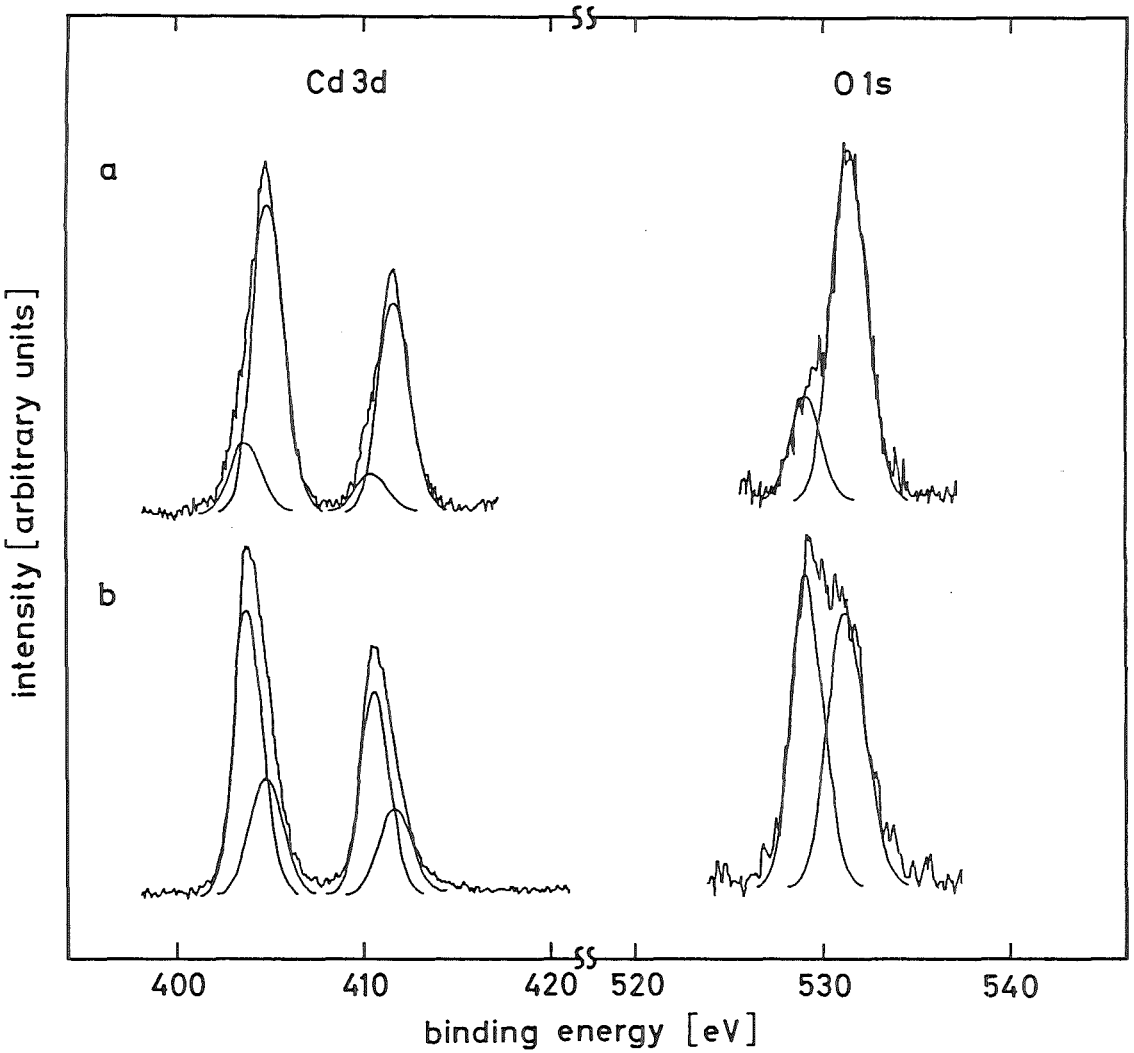

Fig. 11: XPS Cd 3d and O 1s spectra of aerosol sample no. 1 (melting charge temperature 1275 °C) after background and X-ray satellite subtraction together with the Gaussian single components used to fit the original data. The left Gaussian peaks are each attributed to cadmium(II)oxide, the others to cadmium(II)hydroxide.
a) before sputtering; b) after 15 minutes sputtering

Sputtering leads to significant changes in the peak shapes of Cd 3d and O 1s as shown in Fig. 11 b for the aerosol particle surface after 15 minutes sputtering. There are still two components but the relative intensities change drastically in both, the Cd 3d and the O 1s spectra by favoring the low binding energy constituent relative to the second one. Further sputtering does not lead to additional changes in the XPS spectra. Table 5 summarizes the relevant energy values of cadmium and oxygen. The binding energy values correspond to the positions of the resolved Gaussian components of each peak. The energies of the unsputtered sample are given relative to the C 1s level of the surface contamination. Since sputtering led to a decrease of the C 1s signal intensity and obviously to a binding energy shift, the standard was believed not to be reliable any more. It was, therefore, arbitrarily assumed that the O 1s peak at 529.2 eV binding energy would not change its position with sputtering, and binding energies were referenced to this level. For comparison, Table 5 includes the corresponding data of cadmium hydroxide and cadmium oxide, respectively. The data were evaluated from a cadmium oxide standard, which showed after introduction into the UHV system a surface, which consisted of almost equal contributions of cadmium oxide and hydroxide, as judged from the O 1s peak. Short sputtering led to an almost complete removal of the hydroxide, and subsequent data analysis yielded the values given for CdO in Table 5. These values and the corresponding spectra were then used for a spectra subtraction procedure applied to the original CdO standard surface spectra to determine the energetic parameters of $Cd(OH)_2$. Both data sets agree reasonably with published literature values (17,33,37).

From the values given in Table 5 it must be concluded that the aerosol contains $Cd(OH)_2$ and CdO. The molar ratio of both compounds (given in the last column of Table 5 and calculated from the peak areas of the Cd 3d Gaussian components) indicates that the surface consists mainly of cadmium hydroxide and only small contributions of its oxide. A dehydratization in the ultra-high vacuum (UHV) can be excluded since we do not observe increasing amounts of oxide with a prolonged stay of the sample in the UHV.

Sputtering leads to a relative increase of the oxidic component as can be seen from both, the Cd 3d and O 1s peaks. A steady state is reached already after four minutes of sputtering and is characterized by a molar ratio of CdO to $Cd(OH)_2$ of about two, which can be calculated from the peak areas of the Cd 3d single constituents and, in addition from the relative intensities of the oxide and hydroxide O 1s peaks. The latter case can only be taken as an estimate because of a contribution of indium oxide to the left oxidic peak. This may also explain

Table 5: Spectral Parameters of Cadmium in Aerosol Sample No. 1 after Various Sputtering Times and of Cadmium Hydroxide and Cadmium Oxide Standards

Sample	Sputtering Time [min]	Binding Energy [eV] Cd $3d_{5/2}$	O 1s	Modified Auger Parameter [eV] Cd[a]	O[b]	CdO/ $Cd(OH)_2$
Aerosol[c]	0	405.3	531.7	785.3	-	0.15
		404.1	529.2	-	-	
	4	405.3	531.6	-	-	2.1
		404.3	529.2[d]	786.4	-	
	15	405.3	531.4	-	-	2.1
		404.3	529.2[d]	-	-	
$Cd(OH_2)$[e]	-	405.2	531.1	785.2	1041.9	-
CdO[e]	-	404.1	528.8	786.8	1044.6	-

a) Defined as the sum of Cd $3d_{5/2}$ binding energy and Cd($M_4N_{4,5}N_{4,5}$) kinetic energy.

b) Defined as the sum of O 1s binding energy and O(KLL) kinetic energy.

c) Binding energies of the unsputtered sample given relative to C 1s = 285.0 eV.

d) Taken as internal standard for sputtered aerosol sample (cf. discussion).

e) Binding energies given relative to Au $4f_{7/2}$ = 84.0 eV.

why the binding energy of the left peak differs from that of O 1s in CdO by 0.4 eV. The right hydroxidic oxygen component is shifted to slightly lower binding energy after sputtering. Its binding energy is higher compared to what is expected for $Cd(OH)_2$, but approaches this value with increasing sputtering time. We believe that this effect may be due to the presence of some adsorbed water whose O 1s peak is in general observed at higher binding energy compared to hydroxide oxygen (34,35), but has not been discriminated from the latter in our experiments. Consequently, the actual value of the binding energy depends on the relative amounts of hydroxide and water.

McIntyre et al. (38) and T.J. Chuang et al. (39) have observed the conversion of $Ni(OH)_2$ into the oxide during ion bombardment. If this observation is of general significance, we cannot conclude quantitatively on the contributions of oxide and hydroxide below the original aerosol surface. However, the amount of hydroxide in the steady state corresponds to the minimum fraction of this compound in the aerosol bulk. Its contribution after sputtering is of considerable quantity so that the formation of a surface hydroxide resulting from the surface-near hydrolysis of preformed cadmium oxide containing particles can be ruled out. Both, $Cd(OH)_2$ and CdO must have been formed at an early stage of the aerosol particle formation process.

In addition, the presence of large amounts of cadmium metal can also be ruled out. Even though the Cd 3d binding energy of cadmium metal is almost identical to that of cadmium hydroxide (17) the value of the modified Auger parameter and the ratio of the two resolved O 1s peak components (oxide and hydroxide, respectively), the latter confirming the cadmium peak analysis based on the presence of CdO and $Cd(OH)_2$ alone, exclude the presence of large amounts of the metal. Small amounts, however, will not be detectable in the complex mixture.

3.3 Details of indium speciation

Sputtering of aerosol sample no. 6 (and equally of no. 7) leads to a relative increase of the indium signal intensity (cf. Fig. 9), which is, however, not the only significant change. The indium $M_{4,5}N_{4,5}N_{4,5}$ Auger transition whose shape before sputtering indicates a single compound (indium oxide) shows with increasing sputtering time broadening of its two peaks (M_4NN and M_5NN, respectively), until after 10 minutes an almost unstructured $M_{4,5}N_{4,5}N_{4,5}$ peak shape is achieved (cf. Fig. 12 a). Further sputtering did not lead to additional

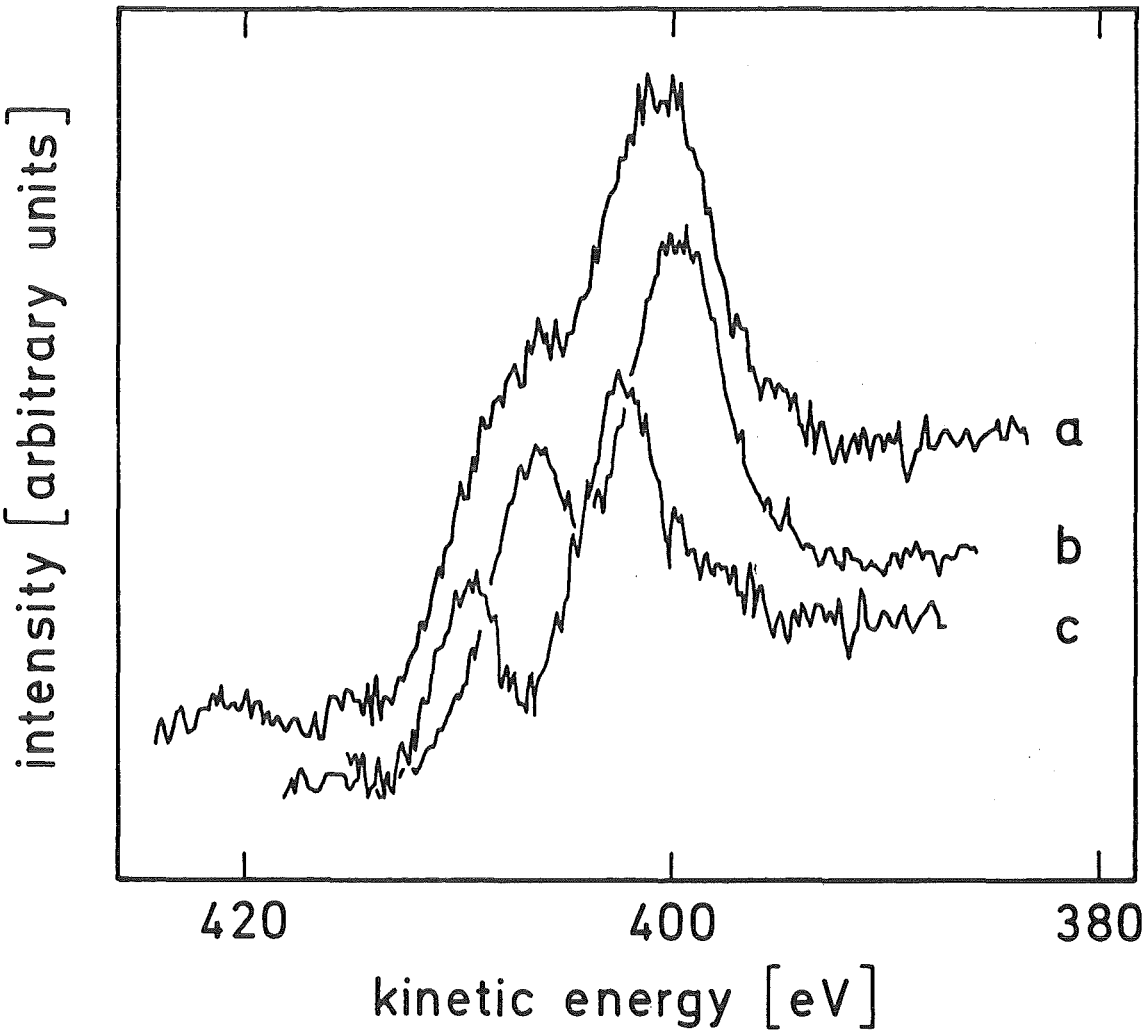

Fig. 12: X-ray induced In($M_{4,5}N_{4,5}N_{4,5}$) Auger transition of aerosol sample no. 6 after ten minutes sputtering. The overall curve (a) can be divided into two components, which are attributed to indium oxide (b) and to indium metal (c).

changes. The multiplet can be resolved into two components, which are attributed to indium oxide and to indium metal (Fig. 12 b and 12 c), respectively. That the indium 3d peak shapes and binding energies remain nearly unchanged (FWHM increased by about 15 %) can be understood, if the small difference in binding energy between indium metal and indium oxides is considered.

Sputtering of a pure indium(III)oxide sample revealed decomposition and the formation of a lower oxide, probably indium(I)oxide, but no complete reduction to indium metal. We, therefore, conclude that indium metal is really present in the aerosol bulk and that it contributes significantly to the total indium amount.

Table 6 lists the binding energies of the In $3d_{5/2}$ and the O 1s photopeaks and the values of the modified Auger parameters of sample no. 6, of the standard In_2O_3 sample and of In_2O_3, In_2O, and In^0 from literature (32). Besides the sputtering effects the data show that it will be fairly difficult to distinguish In_2O_3 and In_2O since the differences in spectral parameters are only small. The measured values of the indium modified Auger parameter of all unsputtered aerosol samples vary between 850.8 and 851.1 eV. For that reason, we have not been able to specify, which oxide has been formed.

3.4 Details of tellurium speciation

Fig. 13 a shows the XPS spectrum of sample no. 6 in the energy region of the tellurium 3d photopeaks. In the spectrum four separate peaks are observed. The leftmost peak belongs to silver (Ag $3p_{3/2}$). The other two main peaks are assigned to tellurium in tellurium dioxide based on the determination of the accurate binding energies, the peak intensity ratio and the spin-orbit coupling constant. The small peak between those two of tellurium dioxide, on the other hand, could in principle result from a photoelectron transition in either tellurium metal (Te $3d_{3/2}$) or chromium metal (Cr $2p_{1/2}$), if the approximate position of this peak and the detection of small amounts of chromium by EPXMA are taken into account. A clear discrimination between the two elements based on the spectra alone is not possible because the second peak of the Te 3d doublet or the chromium 2p doublet, respectively, is hidden under the silver $3p_{3/2}$ photopeak. Nevertheless, the peak position is closer to the value expected for tellurium metal than for chromium metal. In addition, we do not have any indication for the presence of oxidized chromium, and the detection of chromium metal without that of chromium oxide does not seem very likely under the

Table 6: Binding Energies of In $3d_{5/2}$ and O 1s and Modified Auger Parameter α (32) of Various Indium Containing Samples

Sample	Sputtering time [min]	Binding Energy [eV] In $3d_{5/2}$	O 1s	α [eV] In[a]	O[b]
Aerosol no. 6	0	444.3	530.0	850.8	
	4	444.2	529.9	≈ 854.0[c] ≈ 851.0[c]	
	10	444.1	529.8	≈ 854.0[c] ≈ 851.0[c]	
In_2O_3 standard	0	444.3	529.7	850.6	1041.8
	2.5	444.2	529.7	850.7[d]	1041.6
	180	444.2	529.7	851.1[d]	1041.9
In_2O_3[e]	-	444.3	-	850.7	-
In_2O[e]	-	444.3	-	851.1	-
In^o e)	-	444.2	-	854.6	-

a) Defined as the sum of In $3d_{5/2}$ binding energy and In ($M_4N_{4,5}N_{4,5}$) kinetic energy

b) Defined as the sum of O 1s binding energy and O(KLL) kinetic energy

c) Peaks not resolved, energy positions of $M_4N_{4,5}N_{4,5}$ determined from multiplet analysis, cf. Fig. 12

d) Only one $M_{4,5}N_{4,5}N_{4,5}$ Auger transition observable, shape unchanged compared to the unsputtered sample

e) Ref. 32, recalibrated relative to Au $4f_{7/2}$ = 84.0 eV

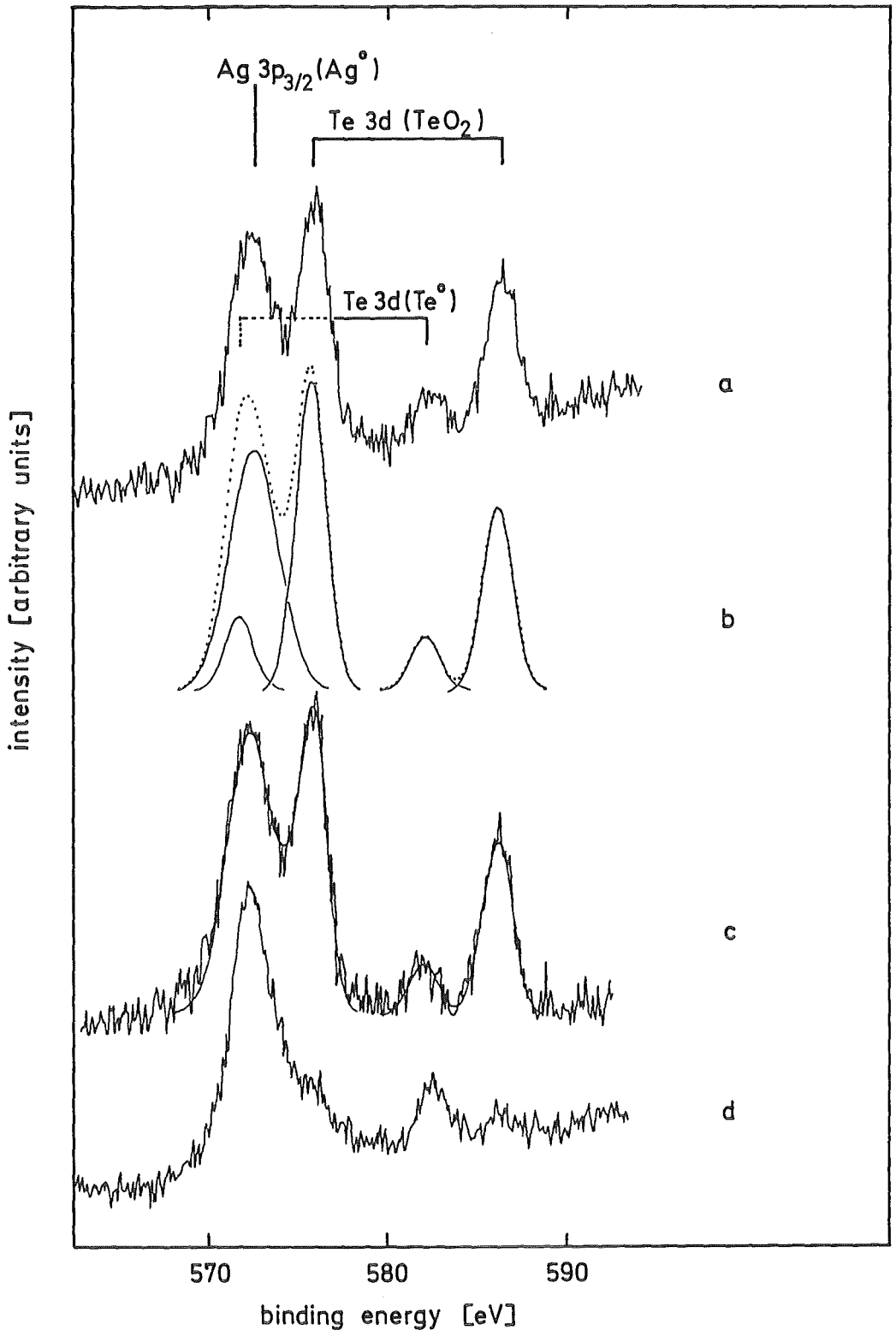

Fig. 13: XPS spectra of aerosol sample no. 6 (melting charge temperature 1900 °C); a) raw data with assignment of components given on top; b) curve synthesis using five Gaussian peaks to fit the experimental spectrum shown under a. The dotted line gives the resulting multiplet; c) comparison of original spectrum (after background and satellite subtraction) with the synthesized multiplet (smooth curve); d) spectrum of the same sample after one minute sputtering showing the almost complete removal of tellurium dioxide.

experimental conditions during the formation of the aerosol samples. It has also been argued above (cf. Table 4) that the amount of chromium, detected by EPXMA, would be below the detection limit of XPS, if it is distributed homogeneously over the whole aerosol material. A detection would only be possible if an enrichment at the surface had occurred. The latter can be ruled out by sputtering the sample, which establishes the presence of the peak at about 584 eV independent of sputtering time with almost unchanged intensity. We, therefore, favor the presence of tellurium rather than chromium metal.

Figs. 13 b and 13 c show the results of a curve synthesis of the spectrum after subtraction of background and of X-ray satellites. The figures show that the fit of the synthesized spectrum to the original data is very good (Fig. 13 c) if it is assumed that silver metal and tellurium metal and dioxide are the only species having photopeaks in this energy region and if the corresponding data (binding energies, relative peak intensities, spin orbit splitting) are used for the synthesis. The close agreement of original and synthesized spectra can be taken as additional evidence for the presence of tellurium metal.

Fig. 13 d shows the XPS spectrum of the same aerosol sample after one minute of argon ion bombardment. The peaks attributed to tellurium dioxide have almost disappeared while the resolved one of tellurium metal is still present with an intensity comparable to the unsputtered surface. Since tellurium dioxide as a bulk compound is not decomposed to the metal under ion bombardment (40,41) the observed behavior indicates that tellurium dioxide is only a surface component of the aerosols. As already stated, further sputtering does not lead to changes of the tellurium metal peak intensity. Taking into account the quick removal of tellurium dioxide it can be concluded that in fact the major amount of tellurium (integrated over the whole aerosol particle volume) is present as metal. It should also be noted that TeO_2 has only been detected in two aerosol samples, but that the metal has been observed in all aerosol samples except the first two ones. Its amount never exceeds about one atomic percent.

Metal tellurides have been discussed as possible chemical species for the release of tellurium (15,42,43). It can be expected that their Te 3d binding energies do not differ significantly from those of tellurium metal and that, therefore, it will be difficult to distinguish tellurides from tellurium metal in XPS.

Summary

The results described in the foregoing discussion apply, due to the relatively low melting charge temperature, to the release behavior of volatile fission products and structural materials during the heat-up phase of a core meltdown accident. Consequently, the release of less volatile materials (e.g. steel constituents, uranium dioxide, Zircaloy constituents) is observed to a negligible extent, if at all. The release process is, therefore, only a section of the whole meltdown process. On the other hand, this has the important advantage to reduce possible spectral interferences, which otherwise could hamper a detailed analysis of the released elements.

One of the important results of the comparison of surface and bulk composition is the fact that at high melting charge temperatures concentration gradients are observed, which are absent at low temperatures. These gradients can be correlated with the condensation temperatures of the vaporized materials. Due to the large differences in condensation temperatures of the participating elements or compounds, those elements with low volatility (Ag, In) condense first after leaving the volatilization zone and form some kind of aerosol nucleus, which afterwards provides a condensation surface for more volatile elements (Cd, Cs, I). It is interesting to note that the small differences in volatility of silver and indium are sufficient to form gradients of their in-depth concentrations. The absence of gradients at low melting charge temperatures can be understood in terms of similar volatilities of the major aerosol constituents and / or if a more or less continuous release and subsequent condensation of the observed elements takes place.

The presence or absence of concentration gradients besides other effects described in the discussion will directly influence the accuracy of the results shown in Figs. 6 to 9. It has been shown, for example, that tellurium dioxide is present at the aerosol particle surface as a very thin layer only. Therefore, its concentration will be overestimated in the upper diagram of Fig. 6 relative to the other constituents. It has been claimed for EPXMA that the relative concentrations of major components will be accurate to within ten relative percent while those of minor constituents may differ by fifty relative percent. Similar accuracies can be assumed for XPS results.

Sputtering may also introduce quantitative changes. However, it could be concluded from the comparison of XPS and EPXMA results that these changes

Table 7: Chemical Speciation of Aerosol Constituents

Element	Chemical Speciation
Ag	metal; iodide[a)]
Cd	hydroxide; oxide
In	oxide; metal[b)]
Te	dioxide[c)]; metal
I	cesium iodide[a)]; silver iodide[a)]
Cs	hydroxide; iodide[a)]

a) from Ref. 21

b) no surface constituent; observable after sputtering

c) only present at the aerosol particle surface

are minor except for sample no. 3, where the expected high sputtering yield of cesium hydroxide led to significant compositional changes.

Table 7 summarizes the results of the chemical speciation of the aerosol constituents, which was evaluated from XPS measurements. The combination of XPS with sputtering revealed in each case a steady state reached already after short sputtering times. The resulting, "new" surface can be assumed to be representative for the bulk composition. This allows to extend the results of XPS, which are primarily only valid for the probed surface-near volume, to the bulk of the samples. However, quantitative information on the chemical composition in contrast to the elemental one is uncertain after sputtering due to the possible induction of chemical changes (e.g. $Cd(OH)_2 \rightarrow CdO$).

It is beyond the scope of this paper to compare our results in detail to thermodynamic predictions concerning the chemical states of elements released during severe nuclear LWR core meltdown accidents (42,43,44). However, it can be stated that both approaches, the experimental and the theoretical one, show agreement for the chemical speciation of certain elements (e.g. cesium hydroxide, indium oxide) but differ for others, (e.g. tellurium dioxide).

Acknowledgment: The authors thank Dr. H. Albrecht and Mr. H. Wild for the aerosol sample preparation and for helpful discussions.

References

1. A. Bayer and F.W. Heuser, Nucl. Saf. 22, 695 (1981)
2. D.O. Campbell, A.P. Malinauskas, and W.R. Stratton, Nucl. Technol. 53, 111 (1981)
3. D. Briggs and J.C. Riviere in "Practical Surface Analysis by Auger and X-ray Photoelectron Spectroscopy", Eds. D. Briggs and M.P. Seah, John Wiley & Sons Ltd., Chichester (1983), p. 87
4. D.M. Hercules and S.H. Hercules, J. Chem. Ed. 61, 483 (1984)
5. T.A. Carlson, "Photoelectron and Auger Electron Spectroscopy", Plenum Press, New York (1975); a) chap. 1, p. 24; b) chap. 5, p. 273
6. D. Briggs, "X-ray Photoelectron Spectroscopy as an Analytical Technique", in "Handbook of X-ray and Ultraviolet Photoelectron Spectroscopy", Heyden London (1977), p. 179
7. R.L. Dod and T. Novakow, "Application of Thermal Analysis and Photoelectron Spectroscopy for the Characterization of Particulate Matter", in "Industrial Applications of Surface Analysis", Eds. L.A. Casper and C.J. Powell, ACS Symposium Series 199, Washington DC (1982)
8. "Characterization of Particles", Ed. K.F.J. Heinrich, NBS Special Technical Publication 533, Washington DC (1980)
9. D.F.S. Natusch, E.R. Denoyer, T.R. Kayser, S.E. Kirton, and D.R. Taylor, AIChE Symp. Ser. 76, 127 (1980)
10. X.B. Cox and R.W. Linton, "XPS Studies of Size Resolved Atmospheric Particles" in "Microbeam Analysis", Ed. K.F.J. Heinrich, San Francisco Press Inc., San Francisco (1982), p. 170
11. G.E. Cabaniss and R.W. Linton, "The In-situ Determination of the Chemistry of PAH on Particle Surfaces", in "Polynuclear Aromatic Hydrocarbons: Chemical Analysis and Biological Fate", Eds. M. Cooke and A.J. Dennis, Batelle Press, Columbus, Ohio (1981), p. 277
12. K.F.J. Heinrich, "Electron Beam X-ray Microanalysis", Van Nostrand Reinhold Company, New York (1981), chap. 9, p. 219
13. S.J.B. Reed, "Electron Mircoprobe Analysis", Cambridge University Press, Cambridge (1975); a) chap. 15, p. 275; b) chap. 15, p. 277; c) Appendix p. 379; d) chap. 1, p. 1; e) chap. 13, p. 236
14. H. Albrecht, V. Matschoss, and H. Wild, Nucl. Technol. 46, 559 (1979)
15. H. Albrecht and H. Wild, "Behavior of I, Cs, Te, Ba, Ag, In, and Cd During Release from Overheated PWR Cores", International Meeting on Light Water Reactor Severe Accident Evaluation, August 28 - September 1, 1983, Cambridge, Mass.

16. H. Albrecht and H. Wild, "Review of the Main Results of the SASCHA Program on Fission Product Release under Core Melting Conditions", ANS Topical Meeting on Fission Product Behavior and Source Term Research, July 15-19, 1984, Snowbird, Utah.
17. D. Briggs and M.P. Seah, Eds., "Practical Surface Analysis by Auger and X-ray Photoelectron Spectroscopy", Appendix 4, p. 477, John Wiley & Sons Ltd., Chichester (1983)
18. J.H. Scofield, J. Electron Spectrosc. Relat. Phenom. 8, 129 (1976)
19. D.A. Shirley, Phys. Rev. B5, 4709 (1972)
20. H. Moers, J.G. Dillard, H. Klewe-Nebenius, G. Kirch, G. Pfennig, and H.J. Ache, Spectrochim. Acta B39, 1563 (1984)
21. H. Moers, J.G. Dillard, H. Klewe-Nebenius, G. Kirch, G. Pfennig, and H.J. Ache, Surf. Interface Anal. 7, 22 (1985)
22. M.P. Seah, "Quantification of AES and XPS", in "Practical Surface Analysis by Auger and X-ray Photoelectron Spectroscopy", Eds. D. Briggs and M.P. Seah, John Wiley & Sons Ltd., Chichester (1983), p. 181
23. C.D. Wagner, Anal. Chem. 49, 1282 (1977)
24. R.S. Swingle II, Anal. Chem. 47, 21 (1975)
25. Vacuum Generators Scientific Ltd., East Grinstead, GB, private communication
26. M.P. Seah and W.A. Dench, Surf. Interface Anal. 1, 2 (1979)
27. J. Gavriolic, "Quantitative Analysis of Small Particles Using Wavelength and Energy Dispersive Systems in an Electron Beam Instrument", in "Characterization of Particles", Ed. K.F.J. Heinrich, NBS Special Technical Publication 533, Washington DC (1980), p. 21
28. J.A. Small, K.F.J. Heinrich, D.E. Newbury, R.L. Myklebust, and C.E. Fiori, "Procedure for the Quantitative Analysis of Single Particles with the Electron Probe", in "Characterization of Particles", Ed. K.F.J. Heinrich, NBS Special Technical Publication 533 (1980), p. 29
29. R. Kelly, Surf. Sci. 90, 280 (1979)
30. D.R. Stull and H. Prophet, JANAF Thermodynamical Tables, 2nd ed., US Government Printing Office, Washington (1971)
31. M.W. Chase, J.L. Curnutt, A.T. Hu, H. Prophet, A.N. Syvrud, and L.C. Walker, J. Phys. Chem. Ref. Data 3, 311 (1974)
32. C.D. Wagner, L.H. Gale, R.H. Raymond, Anal. Chem. 51, 466 (1979)
33. C.D. Wagner, W.M. Riggs, L.E. Davis, and J.F. Moulder, "Handbook of X-ray Photoelectron Spectroscopy", Ed. G. Muilenberg, Perkin Elmer Corporation, Eden Prairie (1978)
34. J.C. Fuggle, L.M. Watson, and D.J. Fabian, Surf. Sci. 49, 61 (1975)
35. C.D. Wagner, D.A. Zatko, and R.H. Raymond, Anal. Chem. 52, 1445 (1980)
36. S. Hofmann and J. Sanz, J. Trace Microprobe Techn. 1, 213 (1982-83)

37. S.W. Gaarenstroom and N. Winograd, J. Chem. Phys. 67, 3500 (1977)
38. N.S. McIntyre and D.G. Zetaruk, J. Vac. Sci. Technol. 14, 181 (1977)
39. T.J. Chuang, C.R. Brundle, and K. Wandelt, Thin Solid Films 53, 19 (1978)
40. H.M. Naguib and R. Kelly, Rad. Effects 25, 79 (1975)
41. H. Moers, unpublished results
42. D. Cubicciotti and B.R. Sehgal, Nucl. Technol. 65, 266 (1984)
43. D. Cubicciotti, Pure Appl. Chem. 57, 1 (1985)
44. R. Hahn and H.J. Ache, Nucl. Technol. 67, 407 (1984)